Curcumin-loaded PEG-PDLLA nanoparticles for attenuating palmitate-induced oxidative stress and cardiomyocyte apoptosis through AMPK pathway

JINGYI ZHANG[1*], YING WANG[2*], CUIYU BAO[1], TAO LIU[1], SHUAI LI[1], JIAXI HUANG[1], YING WAN[3] and JING LI[1]

[1]Hubei Province Key Laboratory on Cardiovascular, Cerebrovascular and Metabolic Disorders, Hubei University of Science and Technology, Xianning, Hubei 437100; [2]Changchun People's Hospital, Changchun, Jilin 130021; [3]College of Life Science and Technology, Huazhong University of Science and Technology, Wuhan, Hubei 430074, P.R. China

Received October 25, 2018; Accepted June 4, 2019

DOI: 10.3892/ijmm.2019.4228

Abstract. Curcumin (CUR) has the ability to attenuate oxidative stress in the myocardium and to protect the myocardium from lipotoxic injury owing to its lipid-reducing properties. However, the use of CUR is limited due to its hydrophobicity and instability. In this study, CUR-loaded nanoparticles (CUR NPs) were developed using an amphiphilic copolymer, monomethoxy poly (ethylene glycol)-b-poly (DL-lactide), as a vehicle material. CUR NPs with high drug loading and small size were prepared under optimized conditions. The effects of CUR NPs on palmitate-induced cardiomyocyte injury were investigated and the possible protective mechanism of CUR NPs was also examined. It was found that CUR NPs were able to control the release of CUR and to deliver CUR to H9C2 cells, and they could prevent palmitate-treated H9C2 cells from apoptosis. In addition, CUR NPs could regulate the Bax and Bcl-2 levels of palmitate-treated H9C2 cells back to their respective normal levels. A prospective mechanism for the function of CUR NPs is that they may activate the AMP-activated protein kinase (AMPK)/mammalian target of rapamycin complex-1/p-p70 ribosomal protein S6 kinase signaling pathway, regulate the expression of downstream proteins and resist the palmitate-induced cardiomyocyte injury. Results suggest that CUR NPs can attenuate palmitate-induced oxidative stress in cardiomyocytes and protect cardiomyocytes from apoptosis through the AMPK pathway. In view of the safety and efficiency of these CUR NPs, they have potential for application in protecting the myocardium from lipotoxic injury.

Correspondence to: Professor Ying Wan, College of Life Science and Technology, Huazhong University of Science and Technology, 1037 Loyu Road, Wuhan, Hubei 430074, P.R. China
E-mail: ying_wan@hust.edu.cn

Professor Jing Li, Hubei Province Key Laboratory on Cardiovascular, Cerebrovascular and Metabolic Disorders, Hubei University of Science and Technology, 88 Xianning Avenue, Xianning, Hubei 437100, P.R. China
E-mail: lijing790629@163.com

*Contributed equally

Key words: curcumin, nanoparticles, palmitate, cardiomyocyte, H9C2, oxidative stress, apoptosis, AMP-activated protein kinase pathway

Introduction

Diabetes and obesity are both associated with lipotoxic cardiomyopathy exclusive of coronary artery disease and hypertension (1-3). Lipotoxicities have become a public health concern and are responsible for a significant portion of clinical cardiac disease (4-7). These abnormalities may be the result of a toxic metabolic shift to more fatty acid and less glucose oxidation with concomitant accumulation of toxic lipids (5). Lipids can directly alter cellular structures and activate downstream pathways, leading to toxicity (5). Previous data have implicated fatty acids, fatty acyl coenzyme A, diacylglycerol, and ceramide in cellular lipotoxicity, which may be caused by apoptosis, defective insulin signaling, endoplasmic reticulum stress, activation of protein kinase C, mitogen associated protein kinase activation, or modulation of peroxisome proliferator-activated receptors (5). Free fatty acids (FFAs), a key of type fat originating from the adipose tissue in the human body, can function as an essential energy provider at their normal level and are able to provide ~70% of adenosine triphosphate to cardiomyocytes (8). A number of studies have revealed that lipid deposition in cardiac tissue would increase provided that the level of FFAs is significantly increased compared with the normal value (9-11). This type of increase in lipid deposition could cause the rise of intracellular active oxygen species (ROS) in cardiomyocytes, commonly called as lipotoxicity and such excessive levels of ROS will in turn result in apoptosis in cardiomyocytes and related cardiac complications (11-14). Therefore, inhibiting the

rise of intracellular ROS in cardiomyocytes would be a viable approach for protecting the myocardium against lipotoxic injury. A previous study on FFAs-induced myocardial injury indicated that AMP-activated protein kinase (AMPK) was able to effectively inhibit the ROS increase in cardiomyocytes by attenuating oxidative stress and concomitantly, prevented the cardiomyocytes from apoptosis (15). With this in mind, it can be envisioned that the lipotoxic myocardial injury could be avoided if certain antioxidants can be used for suppressing the intracellular ROS increase by attenuating oxidative stress and meanwhile, for activating the AMPK pathway in a safe, and effective manner.

Curcumin (CUR) is a hydrophobic polyphenol derivative that is usually extracted from natural herbs and it has diverse pharmacological properties (16-18). In particular, CUR is relatively safe to normal tissues in its therapeutic dose range. CUR has been used as anti-inflammatory, antioxidant and anticancer agents over a long period of time for the treatments of a number of types of diseases, including varied types of cancers, cardiovascular diseases and autoimmune diseases (19-24). A new study reveals that curcumin has the ability to attenuate oxidative stress in the myocardium and can play a protective and therapeutic role in the protection of the myocardium against lipotoxic injury owing to its lipid-lowering properties (25). In another study involving diabetic rats, CUR shows the ability to reduce cardiomyocyte remodeling and relieve cardiac insufficiency (26). Nevertheless, satisfactory pharmaceutical efficacy of CUR is difficult to achieve even though a high dosage is applied because CUR is very hydrophobic, which will lead to its rapid elimination *in vivo*; and in addition, CUR is unstable in an aqueous medium and can be quickly degraded *in vivo* (27,28). Therefore, it is necessary to use suitable carriers to deliver CUR in order to prevent its degradation, enhance its intracellular aggregation and increase its bioavailability.

Nowadays, biocompatible nanoparticles (NPs) with hydrophilic surface properties are frequently used for delivering hydrophobic drugs because these NPs can prolong the *in vivo* circulation of the loaded drugs and thus, increase their efficiency and bioavailability (27,28). In this study, an attempt was made to fabricate a type of CUR-loaded NPs using an amphiphilic copolymer, monomethoxy poly (ethylene glycol)-b-poly (DL-lactide; PEG-PDLLA), as a vehicle material to protect CUR from degradation while enhancing its intracellular accumulation. A model based on palmitate-induced cardiomyocyte injury was used to evaluate the performance of CUR-loaded NPs and it was also examined whether these CUR-loaded NPs had an ability to suppress the intracellular ROS increase by attenuating oxidative stress in cardiomyocytes through an unexplored AMPK pathway.

Materials and methods

Materials. H9C2 cardiomyocytes were procured from the Cell Bank of Type Culture Collection of the Chinese Academy of Sciences. Dulbecco's modified Eagle's medium (DMEM), fetal bovine serum (FBS) and type-II collagenase were purchased from Gibco; Thermo Fisher Scientific, Inc. A malondialdehyde (MDA) assay kit was purchased from Nanjing Jiancheng Bioengineering Institute. The superoxide dismutase (SOD) assay kit was purchased from Dojindo Molecular Technologies, Inc. An ROS assay kit was obtained from Applygen Technologies, Inc. Terminal deoxynucleotidyl transferase dUTP nick end labeling (TUNEL) detection kit was purchased from Roche Diagnostics. Rabbit polyclonal antibodies against Bcl-2, Bcl-2 associated X Protein (Bax), phosphorlyated AMPK (p-AMPK), total AMPK, p-mammalian target of rapamycin complex-1 (p-mTORC1), total mTORC1, p-p70 ribosomal protein S6 kinase (p-p70S6K), total p70S6K and β-actin were purchased from Cell Signaling Technology, Inc. Hybond C membranes and ECL western blot detection kit were purchased from Pierce; Thermo Fisher Scientific, Inc. The MTT assay kit and dorsomorphin (compound C) were purchased from Sigma-Aldrich; Merck KGaA. PEG-PDLLA (PEG, 5 kDa, PDLLA, 10 kDa) was bought from Advanced Polymer Materials Inc. Palmitate and all other reagents were purchased from Sigma-Aldrich; Merck KGaA.

Preparation and characterization of CUR-loaded NPs. CUR-loaded NPs were prepared following a method described elsewhere (29). In brief, CUR (1 mg) and PEG-PDLLA (9 mg) were dissolved into tetrahydrofuran (4 ml). This solution was added dropwise into 10 ml distilled water with stirring. The mixture was then dialyzed against water at ambient temperature for 3 days to form NPs and the resulting CUR-loaded NPs were lyophilized for further use. For the sake of simplicity, these CUR-loaded NPs are abbreviated as CUR NPs in the following text.

CUR NPs were dispersed in methanol with ultrasonic treatment and the amount of the extracted CUR was measured using high performance liquid chromatography (Shimadzu LC-20AD) under the following running conditions (Eclipse XDB-C18 column; 150x4.6 mm; 5 μm; Agilent Technologies, Inc.): Dexamethasone acetate was used as internal standard; mobile phase, methanol containing 3 mM mono potassium phosphate and acetic acid (methanol/mono potassium phosphate/acetic acid/water=230/20/2/748, v/v); flow rate, 1.0 ml/min; injection volume, 20 μl; column temperature, 25˚C; and detection wavelength, 227 nm. Drug loading (DL) and loading efficiency (LE) of CUR NPs were calculated using the following formulas:

$$DL\ (\%)=(M_0/M)\ x100\%\ (1)$$

$$LE\ (\%)=(M_0/M_1)\ x100\%\ (2)$$

where M_0 is the mass of CUR encapsulated in NPs, M_1 is the mass of fed CUR and M is the mass of NPs.

The morphology of NPs was viewed using a transmission electron microscope (TEM; Tecnai G2-20). Size distribution of NPs was determined using a dynamic light scattering instrument equipped with a vertically polarized He-Ne laser (Wyatt Technology, Ltd.). zeta potential (ζ) of NPs was measured using a Nano-ZS instrument.

In vitro release. CUR NPs were suspended in 2 ml PBS (pH 7.4) containing Tween-80 (1.0 wt%) and the solution was added to the dialysis bag (MW cutoff: 3.5 kDa) for releasing testing. Briefly, the sealed dialysis bag was introduced into a vial and immersed in 8 ml PBS. The vial was shaken on a

shaking table at a frequency of 1 Hz at 37˚C. At intervals of 2 h, 1 ml of medium was withdrawn and the vial was replenished with the same volume of fresh buffer. The released amount of CUR was determined via UV-vis analysis at a detecting wavelength of 427 nm.

MTT assay. H9C2 cells were expended in DMEM, containing 2.25 g/l glucose and supplementing with 10% FBS, 100 U/ml penicillin, and 100 mg/ml streptomycin in a humidified atmosphere of 5% CO_2 at 37˚C. The expended H9C2 cells were suspended in PBS for further use. H9C2 cells were seeded in 96-well plates at a density of $1x10^5$ cells/well. After incubation overnight, cells were co-cultured with 0-100 μM of CUR or CUR NPs for a period up to 48 h. At the end of the prescribed incubation periods, cells in each well were thoroughly rinsed with PBS and additionally incubated with the MTT agent (0.5 mg/ml) for 4 h at 37˚C. After that, the media were fully discarded and DMSO was added to each well prior to spectrophotometric measurements (570 nm).

Cellular uptake. H9C2 cells were seeded in 6-well culture plates ($2x10^4$ cells/well) in which each well was preset with a cell culture slide and these cells were cultured with complete medium for 24 h. After that, cells were treated with CUR or CUR NPs (CUR equivalent: 100 μM in both cases) for 1 h or 24 h at 37˚C. After removal of the supernatant, cells were washed with PBS for 3 times and fixed in 800 μl formaldehyde solution (4%) at ambient temperature for 20 min. These cells were subsequently stained with DAPI for 10 min at room temperature and imaged by using a confocal laser scanning microscope (CLSM; Olympus Corporation).

Measurement of ROS levels. Dihydroethidium (DHE; Vigorous Biotechnology, Co., Ltd.), a ROS-level indicative fluorescence probe (λ_{ex}=535 nm, λ_{em}=610 nm), was used to detect intracellular superoxide anions. Briefly, H9C2 cells were seeded in 6-well plates ($2x10^4$ cells/well) and cultured with complete medium for 24 h. Cells were then divided into different groups and exposed to palmitate (0.2 mM) or palmitate (0.2 mM)+CUR NPs (CUR equivalent: 100 μM), respectively, for 24 h at 37˚C. Afterwards, cells were washed with cold PBS and further incubated with fresh medium containing 10 μM DHE at 37˚C in the dark for 20 min to perform nuclei staining. The harvested cells were resuspended in PBS at a density of $2x10^7$ cells/ml, transferred to a light-shielded 96-well plate (100 μl cell suspension per well), followed by determination of DHE intensity using a fluorescence microplate reader (Bio-Rad Laboratories, Inc.). Fluorescence microscopy (Olympus Corporation) was also used to observe the intensity of the fluorescent signals.

Determination of major biochemical parameters. MDA and SOD were measured using an MDA assay kit and a SOD activity kit, respectively. MDA acted as an index for indicating the intracellular oxidative stress levels and SOD was served as an indicator for reflecting the extent of attenuation of oxidative stress levels. Briefly, H9C2 cells that were cultured with complete medium for 24 h were divided into different groups and these groups were treated with palmitate (0.2 mM) or palmitate (0.2 mM)+CUR NPs (prescribed CUR equivalent: 40, 80 and 100 μM) for 24 h at 37˚C. The harvested cells were lysed with RIPA lysis buffer (Cell Signaling Technology, Inc.) and the supernatant was collected by centrifugation at 12,000 x g for 10 min at 4˚C. Protein content in the supernatant was detected using a bicinchoninic acid (BCA) kit. In addition, 100 μl supernatant was introduced into a centrifuge tube and an MDA testing solution (200 μl) was added. After being mixed, the mixture was boiled for 15 min and cooled to room temperature, followed by centrifugation at 1,000 x g for 10 min at 4˚C. A total of 200 μl prepared supernatant was added to 96-well plate and the absorbance was measured at 532 nm using a microplate reader (Bio-Rad Laboratories, Inc.).

SOD activity was determined based on its ability to inhibit the oxidation of oxymine by O^{2-}• that was produced from the xanthine/xanthine-oxidase system. The harvested cells were homogenized and the obtained homogenate was centrifuged at 12,000 x g for 10 min at 4˚C. The protein content in supernatant was determined using a BCA kit. To a centrifuge tube, 20 μl of supernatant and 160 μl NBT/enzymatic working solution were added, and mixed at 4˚C for 5 min. The mixture was then added with 20 μl of reaction-initiating working solution, incubated at 37˚C for 30 min. Such produced mixture was detected for its absorbance at 560 nm using the same microplate reader mentioned above.

TUNEL testing. An *in situ* cell death detection kit (Roche Diagnostics) was employed for identifying apoptotic cells *in situ*. H9C2 cells were seeded in 6-well plates and incubated with complete medium for 24 h. They were divided into different groups and treated with palmitate (0.2 mM) or palmitate (0.2 mM)+CUR NPs (CUR equivalent: 100 μM) for 24 h at 37˚C, respectively. The washed cells were subjected to the TUNEL testing following the methods provided by the assay kit supplier. After that, DAPI nucleus staining was performed using the same method described above. Fluorescence intensity (red, TUNEL; and blue, DAPI) was measured with a fluorescence microscope equipped with microscope image analysis software (Olympus Stream v. 1.7; Olympus Corporation) and images were taken using an electronic camera. Apoptosis rate of cells was determined with flow cytometry (Beckman Coulter, Inc.) following a method described in the literature (30).

Western blot analysis. The abrogation effect of CUR NPs on palmitate-induced cardiomyocyte apoptosis was examined via western blot analysis. H9C2 cells cultured with complete medium for 24 h were assigned into different groups and they were treated with palmitate (0.2 mM) or palmitate (0.2 mM)+CUR NPs (CUR equivalent: 100 μM) for 24 h at 37˚C. After that, the washed cells were lysed with RIPA lysis buffer (Cell Signaling Technology, Inc.) for 30 min and cell lysates were collected by centrifugation at 12,000 x g and 4˚C for 15 min. Protein concentrations in cell extracts were determined using the bicinchoninic acid protein assay. Approximately 30-50 μg of protein per sample was separated by SDS-PAGE (8-12%) and transferred to a PVDF membrane. After blocking the membrane with 5% nonfat milk for 1 h at room temperature, the following primary antibodies were used for blotting (all at 1:1,000 dilution): Bcl-2 (cat. no. 15071), Bax (cat. no. 5023), p-AMPK (cat. no. 2535), AMPK (cat. no. 5831),

p-mTORC1 (cat. no. 5536), mTORC1 (cat. no. 2972), p-p70S6K (cat. no. 9209), p70S6K (cat. no. 9202) and β-actin (cat. no. 4970). Primary antibodies were incubated with membranes overnight at 4˚C. The membrane was then incubated with horseradish peroxidase-linked rabbit anti-mouse IgG (cat. no. ab6728; 1:2,000; Abcam) for 2 h at room temperature. Finally, the blots were visualized using a chemiluminescence system and quantified using an image analysis software (GeneTools; SynGene).

To examine the effect of CUR NPs on the regulation of AMPK pathway in cardiomyocytes, compound C, a type of commonly used inhibitor for AMPK pathway, was employed as a competitive inhibitor when CUR NPs were cultured with cardiomyocytes. H9C2 cells cultured with complete medium for 24 h were divided into different groups and these groups were respectively exposed to palmitate (0.2 mM), palmitate (0.2 mM)+CUR NPs (CUR equivalent: 100 μM), palmitate (0.2 mM)+CUR NPs (CUR equivalent: 100 μM)+compound C (10 μM) for 24 h at 37˚C. In the case of compound C involved group, compound C was applied to cells for 1 h prior to palmitate treatment or the treatment of palmitate+CUR NPs. The expression levels of several specific proteins, including Bcl-2, Bax, AMPK, p-AMPK, mTORC1, p-mTORC1, p70S6K and p-p70S6K, were measured using western blot analysis. In all above mentioned H9C2 cell experiments, the untreated cells were used as controls.

Statistical analysis. All experiments were performed a minimum of three times, and the data were analyzed using GraphPad Prism v5 software (GraphPad Software, Inc.). Data are presented as the means ± standard deviation, and were analyzed using one-way analysis of variance followed by Tukey's post-hoc test. $P<0.05$ was considered to indicate a statistically significant difference.

Results

Basic parameters of CUR NPs. In this study, an attempt was made to prepare a type of CUR NPs that have small sizes and high DL as well as rational LE. A preparation of NPs was optimized by mainly focusing on three factors such as size, DL and LE of NPs based on an orthogonal test, and optimal conditions are summarized in the experimental section. Fig. 1A shows a representative TEM image for the optimally prepared CUR NPs, indicating that these NPs exhibited a size <100 nm with good size uniformity. Fig. 1B presents the size of CUR NPs that had an approximate Gaussian distribution character. Average values for several parameters such as mean size, polydispersity index, zeta potential (ζ), DL and LE were calculated and data are listed in Table I. It can be seen from Table I that these CUR NPs had small sizes, nearly neutral surface charge nature and high DL, suggesting that they have potential for practical applications.

Release profile of CUR NPs. Fig. 1C shows the release profile for CUR NPs. The curve exhibits that CUR was released from CUR NPs at fast rates during the first few hours and cumulative amount of the released CUR reached ~40% within 4 h. After that, the release rate of CUR NPs slowed down and entered a plateau region after 12 h release.

Effect of CUR NPs on viability of H9C2 cells. H9C2 cells were treated with varied amounts of CUR NPs for a given period in order to figure out the safe dosage of applicable CUR NPs and the obtained data are presented in Fig. 2. In cases of CUR treatment, the viability of the treated cells was visibly dependent on the applied CUR dose and the treatment time interval. After 24 h CUR treatment, the viability of cells became ~80% or less when the applied CUR dose reached 40 μM or higher; and with respect to 48 h CUR treatment, the CUR dose had to be limited to <20 μM if the cell viability needs to be maintained at ~80% or higher. As for CUR NPs, the treated cells had a viability >90% even though the CUR equivalent was 100 μM and the treatment time period reached 48 h. These results verify that a much higher CUR amount can be applied to H9C2 cells in comparison to the free CUR when NPs are employed as a vehicle.

Cellular uptake assessment. To view the cellular uptake of CUR NPs, H9C2 cells were incubated with CUR or CUR NPs for 1 h or 24 h, respectively and imaged by CLSM for comparison. As shown in Fig. 3, in both cases of 1 and 24 h, the fluorescence intensity of CUR-NPs group was stronger compared with the CUR group. Furthermore, it was found that as incubation time increased, the fluorescence intensity of free molecule CUR was notably weakened, but the fluorescence intensity of intracellular CUR-NPs was not altered significantly. The reason for these results is that the high concentration of free molecule CUR has toxic effects on cardiomyocytes and hence, cells undergo certain apoptosis-related morphological changes such as cell membrane rupture, and free molecule CUR gradually overflows from the cells, resulting in a decrease in intracellular fluorescence intensity. However, CUR-NPs with the same equivalent CUR concentration would not cause any toxicity to cardiomyocytes (Fig. 2) and thus, the intracellular fluorescence intensity corresponding to CUR-NPs is remained strong after 24 h of incubation. These images confirm that the presently developed CUR NPs can greatly enhance the intracellular CUR accumulation.

Resistance effect of CUR NPs on palmitate-induced lipotoxic cell damage. Various amounts of palmitate were incubated with H9C2 cells to examine the palmitate-induced cell damage by measuring cell viability and relevant results are provided in Fig. 4A and B. Under conditions of fixed incubation time, cell viability was found to sharply decrease when the applied palmitate amount was >0.1 mM; and alternatively, the treated cells also had decreased viability after exposure to 0.2 or 0.4 mM palmitate for a period >12 h. These data reveal that palmitate will induce cardiomyocyte damage when the applied palmitate amount or the treatment time period exceeds certain thresholds. Bar-graphs shown in Fig. 4C illustrate that CUR NPs can effectively resist the palmitate-induced cell damage because the cells treated with 0.2 mM palmitate together with various amounts of CUR NPs for 24 h showed ascending cell viability with significant differences when compared with those cells treated with 0.2 mM palmitate only ($P<0.01$). Based on these results, the applied palmitate amount was selected as 0.2 mM for establishing the palmitate-induced cell damage model for the following experiments unless otherwise stated.

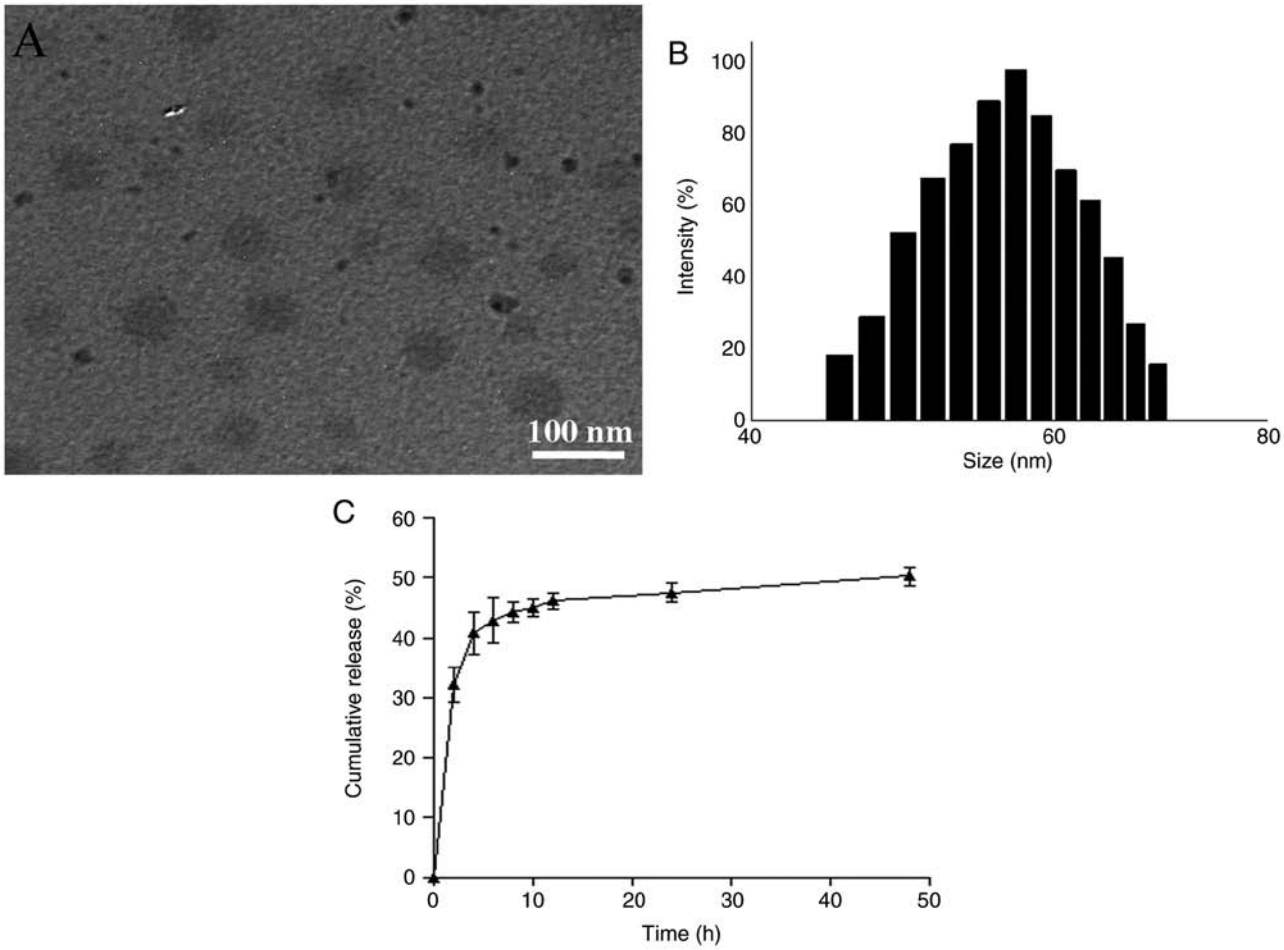

Figure 1. Transmission electron microscopy and size distribution of CUR NPs. (A) Representative image and (B) size distribution of CUR NPs. (C) Cumulative amount of CUR released from CUR NPs. CUR, curcumin; NPs, nanoparticles.

Effects of CUR NPs on palmitate-induced ROS level, MDA content and SOD activity in cells. Palmitate-induced ROS levels were first detected by using DHE as fluorescent probe and results are represented Fig. 5. Images in Fig. 5A denote that the cells treated with palmitate alone show greater red fluorescence compared with the matching control, signifying that the palmitate treatment can lead to a clear increase in intracellular ROS levels. On the other hand, the red fluorescence corresponding to the cells treated with the combination of palmitate and CUR NPs exhibited largely reduced brightness when compared with those cells treated by palmitate only, demonstrating that the use of CUR NPs can prevent intracellular ROS production. Data for DHE fluorescence intensity are depicted in Fig. 5B and the bar-graphs provide quantitative evidence that CUR NPs can significantly inhibit the palmitate-induced increase in ROS levels ($P<0.05$). Fig. 5C and D demonstrate that the palmitate treatment resulted in a big increase in the amount of MDA substance while leading to a significant decrease in SOD activity ($P<0.05$) and such changes are strongly correlated to the rise of intracellular oxidative stress levels. In contrast to these observations, CUR NPs containing a CUR equivalent of 100 μM can inhibit the increase in MDA amount and regulate the SOD activity, allowing these two typical indexes to be back to the normal cellular levels.

Abrogation effect of CUR NPs on palmitate-induced cell apoptosis. Fig. 6A shows that the palmitate-treated cells exhibited greater fluorescence compared with the matching with control (see middle column) and the fluorescence brightness associated with the cells treated with the combination of palmitate, and CUR NPs was largely reduced. The results were consistent with TUNEL positive/negative image data (Fig. S1). The fluorescence intensity of the PA group was close to that of positive control group and that of PA+CUR NPs group was close to that of the negative control group. The quantitative results presented in Fig. 6B demonstrate that CUR NPs were able to completely inhibit the palmitate-induced increase in apoptosis levels.

Possible mechanism for CUR NPs to protect cells from palmitate-induced damage. The AMPK pathway plays an important role in regulating cellular survival, oxidative stress and apoptosis (15). The amount of AMPK and p-AMPK as well as the key downstream proteins (p-mTORC1 and p-p70S6K) was respectively measured for exploring their responses to different treatments involving palmitate, the combination of palmitate and CUR NPs and an AMPK inhibitor (compound C), and the results are presented in Fig. 7. In principle, AMPK is a metabolic fuel gauge and the activation of AMPK acts to maintain cellular energy stores by switching on catabolic pathways that

Table I. Parameters of CUR NPs.

Sample name	Mean size (nm)	Polydispersity index	ζ (mV)	Drug loading (wt%)	Loading efficiency (%)
CUR NPs	57.09±4.52	0.19	0.44±0.018	8.81±0.92	82.3±3.71

CUR, curcumin; NPs, nanoparticles.

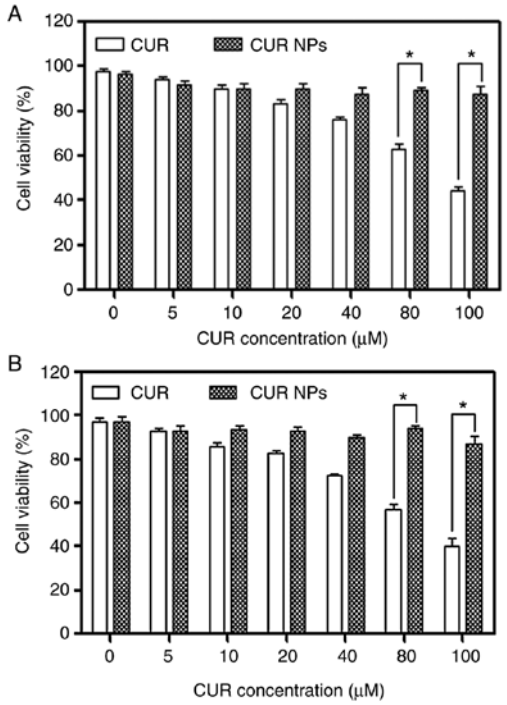

Figure 2. Cytotoxic effects of CUR and CUR NPs on H9C2 cells. Viability of H9C2 cells treated with varied amounts of CUR and CUR NPs for (A) 24 and (B) 48 h, respectively. *P<0.05. CUR, curcumin; NPs, nanoparticles.

initiate ATP production (15). p-AMPK at its normal level can inhibit the activity of downstream p-mTORC1 and p-p70S6K, thereby triggering the ATP production process to maintain the dynamic balance between supply and demand for cellular energy. However, under pathological conditions such as hyperlipidemia, p-AMPK appears to decrease and elevates the levels of p-mTORC1 and p-p70S6K, which will in turn cause a cellular energy imbalance and result in cell damage or apoptosis. Bands matching the palmitate-treated group, as shown in Fig. 7A, registered a clear decrease in p-AMPK, accompanied by increases in levels of both p-mTORC1 and p-p70S6K, although the AMPK, mTORC1 and p70S6K expression remained nearly unchanged in comparison with the control; and on the other hand, the bands for the group treated with the combination of palmitate and CUR NPs demonstrated that p-AMPK, p-mTORC1 and p-p70S6K returned to their respective normal levels. Data presented in Fig. 7B-D indicated that CUR NPs were able to resist the abnormal changes in the levels of p-AMPK, p-mTORC1 and p-p70S6K. In particular when compound C was applied, the resistant effects of CUR NPs on the abnormal changes of these three proteins would be eliminated. These results suggest that CUR NPs can protect cardiomyocytes from lipotoxic injury through the AMPK pathway.

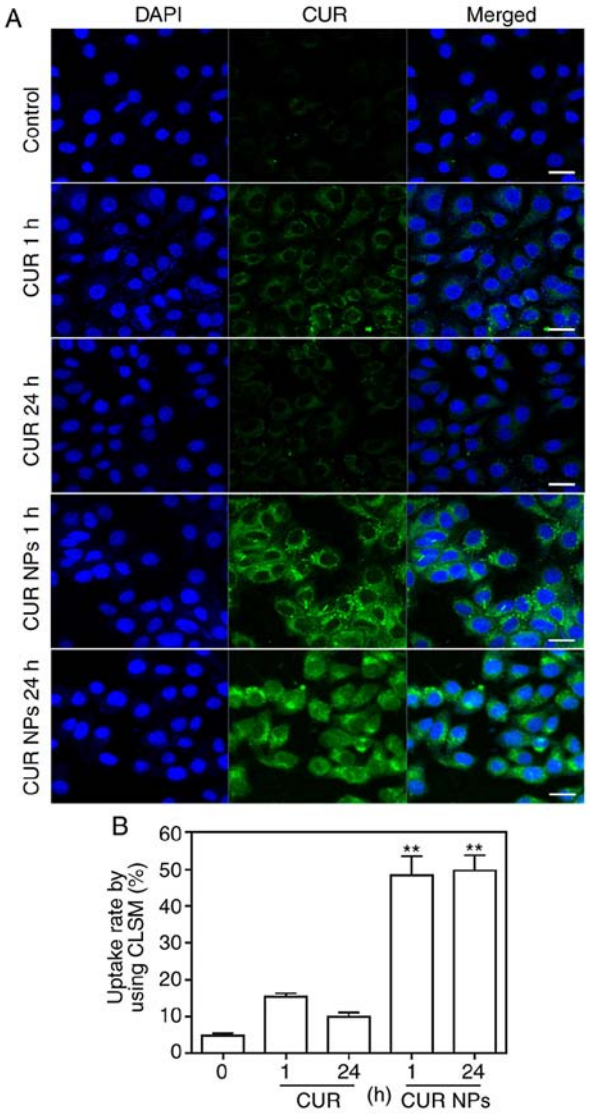

Figure 3. Cell uptake of CUR and CUR NPs on H9C2 cells. (A) Confocal laser scanning microscope images of H9C2 cells treated with CUR and CUR NPs for 1 and 24 h, respectively (CUR equivalent: 100 μM; scale bar: 50 μm). (B) Fluorescence intensity of H9C2 cells treated with CUR and CUR NPs for 1 and 24 h, respectively (CUR equivalent: 100 μM). Quantitative determination of fluorescence intensity. **P<0.01 vs. untreated control. CUR, curcumin; NPs, nanoparticles.

Resistant effect of CUR NPs on palmitate-induced cell apoptosis via AMPK pathway. A total of two key regulatory proteins, Bax and Bcl-2, were further measured using western blotting to examine how they respond to the treatment of CUR NPs and results are presented Fig. 8. Bands for Bax and Bcl-2 in Fig. 8A indicate that the palmitate-treated cells had lower Bcl-2 levels but increased Bax levels compared with the

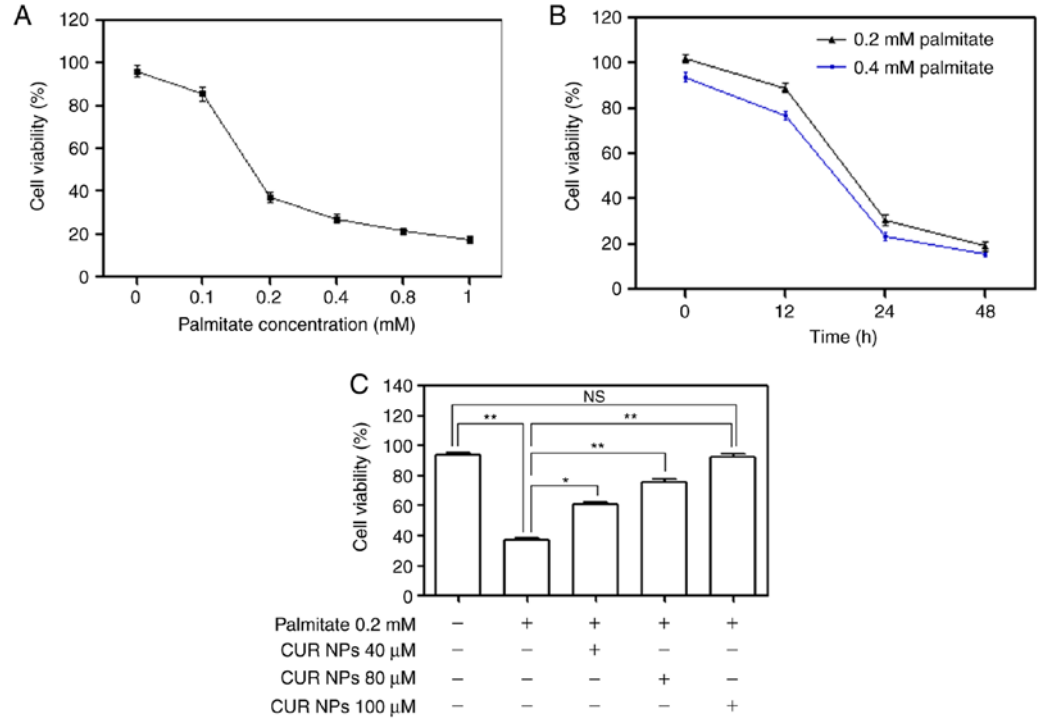

Figure 4. Viability of H9C2 cells treated with palmitate alone and the combination of palmitate and CUR NPs. (A) Palmitate-concentration dependency of cell viability (culture time: 24 h). (B) Time dependency of cell viability. (C) Viability of cells treated with varied formulations (culture time: 24 h). *P<0.05; **P<0.01; NS, no significance; CUR, curcumin; NPs, nanoparticles.

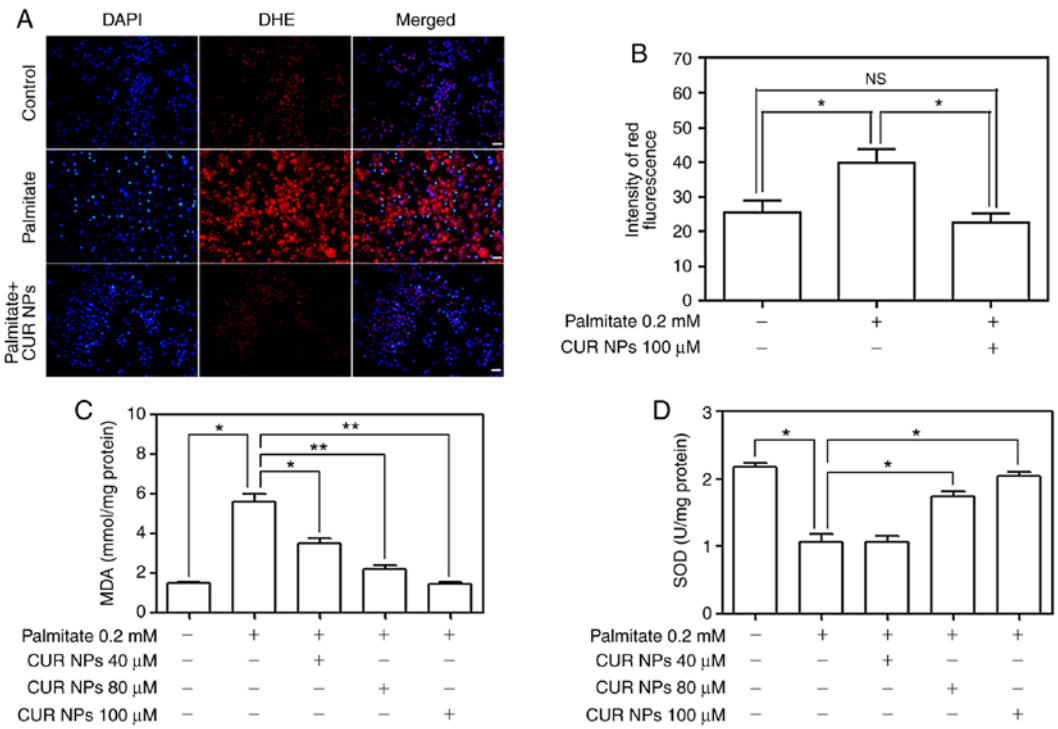

Figure 5. Fluorescence images and major biochemical parameters of H9C2 cells treated with palmitate alone and the combination of palmitate and CUR NPs (culture time: 24 h). (A) Representative images of cells stained with DAPI and DHE (CUR equivalent: 100 μM; scale bar: 20 μm). (B) Fluorescence intensity of DHE. (C) MDA levels in cells. (D) SOD activity in cells. *P<0.05 and **P<0.01; NS, no significance; CUR, curcumin; NPs, nanoparticles; DHE, dihydroethidium; MDA, malondialdehyde; SOD, super oxide dismutase.

control and the cells treated with the combination of palmitate, and CUR NPs exhibited Bcl-2 and Bax levels similar to the control. Considering the fact that the Bcl-2 protein is indicative of the resistance to cell apoptosis while the Bax protein pro-apoptotic, the correct ratio between Bcl-2 and Bax is a crucial factor for cell survival. It can be seen from Fig. 8B

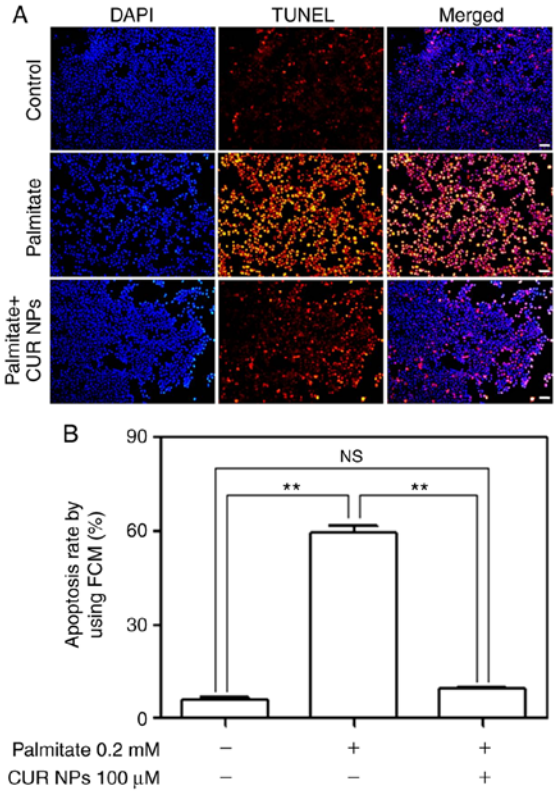

Figure 6. Effect of CUR NPs on palmitate-induced H9C2 cell apoptosis. (A) Representative images of cells (CUR equivalent: 100 μM; scale bar: 20 μm). (B) Quantitative determination of apoptosis rate. **P<0.01; NS, no significance; CUR, curcumin; NPs, nanoparticles.

that the Bcl-2/Bax ratio for the palmitate-treated cells was ~3-fold lower compared with the control, implying that these cells underwent apoptosis. On the other hand, the cells treated with the combination of palmitate and CUR NPs exhibited a Bcl-2/Bax ratio similar to that of the control (P>0.005), demonstrating that the use of CUR NPs can completely inhibit the palmitate-induced apoptosis. However, the Bcl-2/Bax ratio for the group treated with the combination of palmitate, CUR NPs and compound C was greatly reduced to a level similar to palmitate-treated group.

Discussion

Cardiovascular disease is one of the leading causes of death in the world (31). Myocardial infarction, a kind of acute and fatal heart disease, is found to be directly and strongly connected hyperlipidemia that causes atherosclerosis, and in turn, results in a variety of blood vessel related diseases (31). Several studies indicate that hyperlipidemia directly participates in the pathogenesis of high fat-induced cardiac injury in both the human body and experimental animals by promoting the formation of excessive oxidative stress in the heart, and in turn, resulting in cardiomyocyte apoptosis (31-33). In the case of hyperlipidemia, a typical indicator of the rise of oxidative stress in the heart, it is closely linked to the overproduction of ROS and a damaged antioxidant defense system (34), and the disrupted balance between ROS generation and the ROS scavenging system will result in intracellular formation and accumulation of superoxide ions, leading to dysfunction and cell damage (35). Considering that the elevated ROS levels cause strong injurious effects on hyperlipidemia patients, nowadays, various types of antioxidant agents have been investigated for their potential in the treatment of hyperlipidemia (36).

CUR has been used a natural cardioprotective agent because it can eradicate the excessive amounts of ROS and enhance antioxidant defense due to its demonstrated antioxidant properties (37). In the present study, CUR was loaded into NPs in order to protect it from degradation while improving its therapeutic efficiency. Results presented above confirm that the CUR NPs containing a CUR equivalent of 100 μM are able to attenuate oxidative stress in cardiomyocytes and fully resist palmitate-induced cardiomyocyte apoptosis.

The occurrence of hyperlipidemia can be correlated to multiple factors that can act individually or in combination. These factors include superoxide generation from NADPH oxidases (38), oxidative phosphorylation (39), abnormal level of protein kinase C (40) and the activation of polyol, and hexosamine pathways (41). Recent studies reveal that the AMPK pathway can play a critical role in regulating the pathophysiological development of hyperlipidemia and co-morbidities (42,43).

AMPK is known to be a major intracellular protein kinase and it can regulate not only cellular metabolism involving fatty acids and glucose but also anti-apoptotic processes (44). In the case of cardiomyocytes, impaired intracellular metabolism will cause an inadequate energy supply, which would disturb cellular homeostasis and result in irregular contraction of myocardium (45). For this reason, stimulation of AMPK, a key member of well-known cell survival pathways, is believed to be feasible for protecting the myocardium through improved energy utilization, enhanced mitochondrial biogenesis and inhibiting cell apoptosis (46). A recent study suggests that pharmacological activation of AMPK can prevent palmitate-induced mitochondrial fragmentation and dysfunction in endothelial cells (47). Based on these reported results, the present study intends to discover whether CUR NPs can also stimulate AMPK to protect myocytes from lipotoxic injury and also, examine the prospective relationship between AMPK activation and lipotoxic injury of cardiomyocytes.

Although several studies have been performed to activate the AMPK pathway using CUR and the relevant effects on the protection of adipocytes, endothelial cells and cardiomyocytes have been examined (48-50), the general mechanism for CUR to activate the AMPK pathway is still unclear. In the case of endothelial cells, an alternative mechanism is that CUR regulates uncoupling protein 2 and activates the AMPK pathway by inhibiting excessive ATP production in endothelial cells (49). In the present study, besides the achieved improvements on greatly enhanced intracellular accumulation of CUR NPs and strong resistance effect of CUR NPs on the palmitate-induced cardiomyocyte apoptosis, the AMPK/mTORC1/p70S6K pathway in CUR NP treated cardiomyocytes, which is different from other pathways mentioned in the literature and has not been explored so far to the best of our knowledge, was explored in order to find out an alternative mechanism. Under the present experimental conditions, CUR NPs are able to suppress p-mTORC1 and p-p70S6K through promoting the rise of p-AMPK back

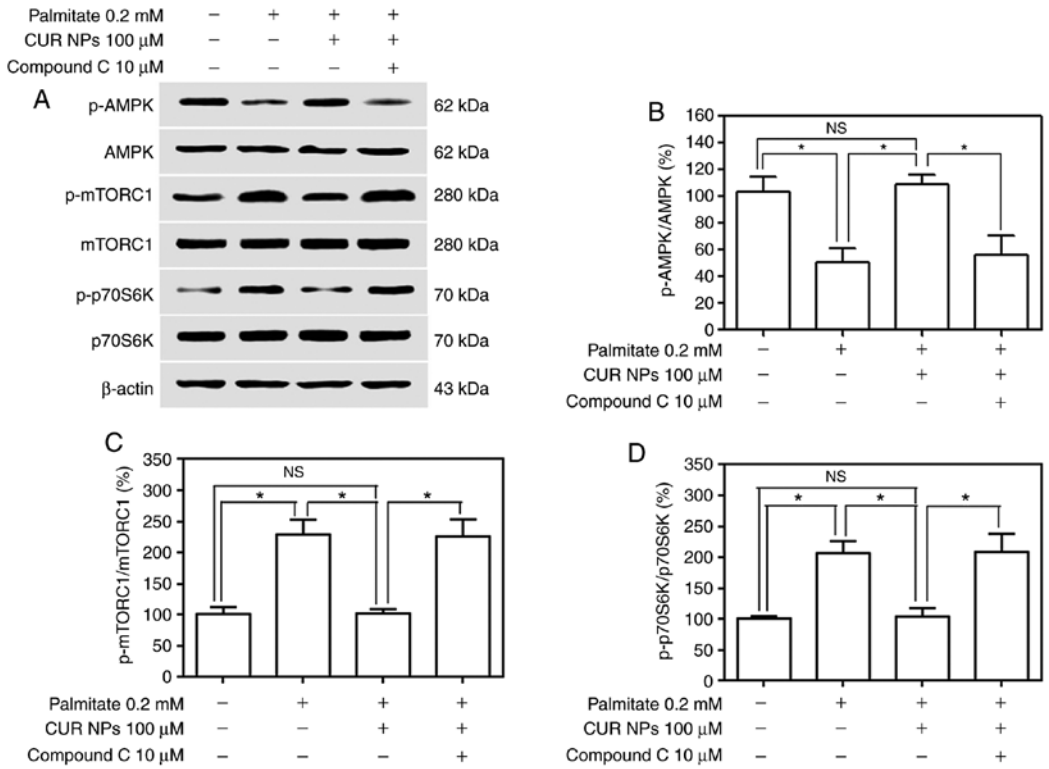

Figure 7. Effect of CUR NPs on regulation of the AMPK pathway in H9C2 cells. (A) Representative bands of p-AMPK, AMPK, p-mTORC1, mTORC1, p-p70S6K and p70S6K (inner reference: β-actin). (B) Quantitative determination of p-AMPK/AMPK ratio. (C) Quantitative determination of p-mTORC1/mTORC1 ratio. (D) Quantitative determination of p-p70S6K/p70S6K ratio. *P<0.05; NS, no significance; CUR, curcumin; NPs, nanoparticles; AMPK, AMP-activated protein kinase; p-AMPK, phosphorylated AMPK; p-mTORC1, phosphorylated mammalian target of rapamycin complex-1C1; p-p70S6K, phosphorylated p70 ribosomal protein S6 kinase.

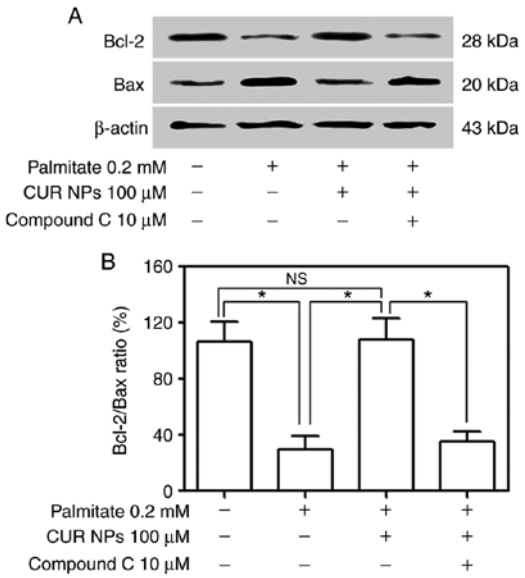

Figure 8. Effect of CUR NPs on the expression of Bax and Bcl-2 proteins in H9C2 cells. (A) Representative bands of Bax and Bcl-2 (inner reference: β-actin). (B) Quantitative determination of Bcl-2/Bax ratio. *P<0.05; NS, no significance; CUR, curcumin; NPs, nanoparticles; Bax, Bcl-2 associated X Protein.

to its normal level, and therefore, protect cardiomyocytes from palmitate-induced lipotoxicity.

It is known that the Bax protein plays a crucial role in mitochondrion-mediated apoptosis and on the other hand, Bcl-2, a kind of antiapoptotic protein, can effectively prevent Bax oligomerization (51). A relatively stable balance between Bax and Bcl-2 is a key factor for maintaining the normal state of cardiomyocytes (51). This effect of CUR NPs is blocked when compound C, a typical inhibitor for AMPK pathway, is applied. Moreover, the regulatory effects of CUR NPs on the expression of Bax and Bcl-2 will also be blocked when AMPK pathway is inhibited by compound C. Based on all observations mentioned in this study, it can be deduced that CUR NPs may activate the AMPK/mTORC1/p70S6K signaling pathway, regulate the expression of downstream proteins and resist the palmitate-induced cardiomyocyte injury.

In conclusion, a type of CUR-loaded NPs with necessitated drug-loading and suitable sizes was successfully prepared, and these NPs showed definite ability to administrate the CUR release in a sustainable manner over a period of ~12 h. These NPs had much higher safety in comparison to free CUR and in addition, were capable of greatly enhancing the intracellular CUR accumulation in cardiomyocytes. They were found to be able to inhibit the rise of intracellular ROS levels and resist palmitate-induced cardiomyocyte apoptosis. A possible mechanism for these NPs to play their roles in cardiomyocyte protection is that the sustained release of CUR can attenuate palmitate-induced oxidative stress in cardiomyocytes and concomitantly, activate the AMPK pathway by regulating the expression of several specific proteins to their respective normal levels. Results suggest that the presently developed CUR-loaded NPs have potential in preventing myocardium from lipotoxic injury. The present studies are focused on the

protective effects of CUR NPs against the palmitate-induced injuries in cardiomyocytes *in vitro*. Some investigations based on the animal model are now in progress and they may be used to further demonstrate the protective effects of CUR NPs on cardiomyocytes *in vivo*.

Acknowledgements

The authors would like to thank Miss Wei Zhang of Changchun Institute of Applied Chemistry, Chinese Academy of Sciences, for providing technical guidance for the synthesis of nanoparticles.

Funding

The present study was supported by the National Natural Science Foundation of China (project no. 51703055), the Jilin Province Science and Technology Development Plan Project (project no. 20170204011YY), the Hubei Natural Science Foundation (grant no. 2017CFB699), the Hubei Science and Technology College Diabetes Special Fund (grant no. 2016-18XZ09) and the Hubei University of Science and Technology School Development Project (grant no. 2016-18X042).

Availability of data and materials

All data generated or analyzed during this study are included in this published article.

Authors' contributions

JZ and JL conceived and designed the study. JZ, YWang, CB, TL, SL, JH and JL performed the experiments. JZ, YWan and JL wrote the paper. JL reviewed and edited the manuscript. All authors read and approved the manuscript.

Ethics approval and consent to participate

Not applicable.

Patient consent for publication

Not applicable.

Competing interests

The authors declare that they have no competing interests.

References

1. Kim J, Joo S, Eom GH, Lee SH, Lee MA, Lee M, Kim KW, Kim DH, Kook H, Kwak TH and Park WJ: CCN5 knockout mice exhibit lipotoxic cardiomyopathy with mild obesity and diabetes. PLoS One 13: e0207228, 2018.
2. Pulinilkunnil T, Kienesberger PC, Nagendran J, Waller TJ, Young ME, Kershaw EE, Korbutt G, Haemmerle G, Zechner R and Dyck JR: Myocardial adipose triglyceride lipase overexpression protects diabetic mice from the development of lipotoxic cardiomyopathy. Diabetes 62: 1464-1477, 2013.
3. Jeong MH, Tran NK, Kwak TH, Park BK, Lee CS, Park TS, Lee YH, Park WJ and Yang DK: β-Lapachone ameliorates lipotoxic cardiomyopathy in acyl CoA synthase transgenic mice. PLoS One 9: e91039, 2014.
4. Walls SM, Cammarato A, Chatfield DA, Ocorr K, Harris GL and Bodmer R: Ceramide-protein interactions modulate ceramide-associated lipotoxic cardiomyopathy. Cell Rep 22: 2702-2715, 2018.
5. Drosatos K and Schulze PC: Cardiac lipotoxicity: Molecular pathways and therapeutic implications. Curr Heart Fail Rep 10: 109-121, 2013.
6. Law BA, Liao X, Moore KS, Southard A, Roddy P, Ji R, Szulc Z, Bielawska A, Schulze PC and Cowart LA: Lipotoxic very-long-chain ceramides cause mitochondrial dysfunction, oxidative stress, and cell death in cardiomyocytes. FASEB J 32: 1403-1416, 2018.
7. Pillutla P, Hwang YC, Augustus A, Yokoyama M, Yagyu H, Johnston TP, Kaneko M, Ramasamy R and Goldberg IJ: Perfusion of hearts with triglyceride-rich particles reproduces the metabolic abnormalities in lipotoxic cardiomyopathy. Am J Physiol Endocrinol Metab 288: E1229-E1235, 2005.
8. Malfitano C, de Souza Junior AL, Carbonaro M, Bolsoni-Lopes A, Figueroa D, de Souza LE, Silva KA, Consolim-Colombo F, Curi R and Irigoyen MC: Glucose and fatty acid metabolism in infarcted heart from streptozotocin-induced diabetic rats after 2 weeks of tissue remodeling. Cardiovasc Diabetol 14: 149, 2015.
9. Carpentier AC: Abnormal myocardial dietary fatty acid metabolism and diabetic cardiomyopathy. Can J Cardiol 34: 605-614, 2018.
10. Mangolim AS, Brito LAR and Nunes-Nogueira VS: Effectiveness of testosterone therapy in obese men with low testosterone levels, for losing weight, controlling obesity complications, and preventing cardiovascular events: Protocol of a systematic review of randomized controlled trials. Medicine (Baltimore) 97: e0482, 2018.
11. Son NH, Yu S, Tuinei J, Arai K, Hamai H, Homma S, Shulman GI, Abel ED and Goldberg IJ: PPARγ-induced cardiolipotoxicity in mice is ameliorated by PPARα deficiency despite increases in fatty acid oxidation. J Clin Invest 120: 3443-3454, 2010.
12. Nakamura H, Matoba S, Iwai-Kanai E, Kimata M, Hoshino A, Nakaoka M, Katamura M, Okawa Y, Ariyoshi M, Mita Y, *et al*: p53 promotes cardiac dysfunction in diabetic mellitus caused by excessive mitochondrial respiration-mediated reactive oxygen species generation and lipid accumulation. Circ Heart Fail 5: 106-115, 2012.
13. Finck BN, Han X, Courtois M, Aimond F, Nerbonne JM, Kovacs A, Gross RW and Kelly DP: A critical role for PPARalpha-mediated lipotoxicity in the pathogenesis of diabetic cardiomyopathy: Modulation by dietary fat content. Proc Natl Acad Sci USA 100: 1226-1231, 2003.
14. Britto RM, Silva-Neto JAD, Mesquita TRR, Vasconcelos CML, de Almeida GKM, Jesus ICG, Santos PHD, Souza DS, Miguel-Dos-Santos R, de Sá LA, *et al*: Myrtenol protects against myocardial ischemia-reperfusion injury through antioxidant and anti-apoptotic dependent mechanisms. Food Chem Toxicol 111: 557-566, 2018.
15. Guo S, Yao Q, Ke Z, Chen H, Wu J and Liu C: Resveratrol attenuates high glucose-induced oxidative stress and cardiomyocyte apoptosis through AMPK. Mol Cell Endocrinol 412: 85-94, 2015.
16. Lu CW, Hao JL, Yao L, Li HJ and Zhou DD: Efficacy of curcumin in inducing apoptosis and inhibiting the expression of VEGF in human pterygium fibroblasts. Int J Mol Med 39: 1149-1154, 2017.
17. Mujtaba T, Kanwar J, Wan SB, Chan TH and Dou QP: Sensitizing human multiple myeloma cells to the proteasome inhibitor bortezomib by novel curcumin analogs. Int J Mol Med 29: 102-106, 2012.
18. Chen Z, Xue J, Shen T, Mu S and Fu Q: Curcumin alleviates glucocorticoid-induced osteoporosis through the regulation of the Wnt signaling pathway. Int J Mol Med 37: 329-338, 2016.
19. Mohajeri M and Sahebkar A: Protective effects of curcumin against doxorubicin-induced toxicity and resistance: A review. Crit Rev Oncol Hematol 122: 30-51, 2018.
20. Santezi C, Reina BD and Dovigo LN: Curcumin-mediated photodynamic therapy for the treatment of oral infections-a review. Photodiagnosis Photodyn Ther 21: 409-415, 2018.
21. Hosseini A and Hosseinzadeh H: Antidotal or protective effects of curcuma longa (turmeric) and its active ingredient, curcumin, against natural and chemical toxicities: A review. Biomed Pharmacother 99: 411-421, 2018.
22. Gawde KA, Sau S, Tatiparti K, Kashaw SK, Mehrmohammadi M, Azmi AS and Iyer AK: Paclitaxel and di-fluorinated curcumin loaded in albumin nanoparticles for targeted synergistic combination therapy of ovarian and cervical cancers. Colloid Surf B Biointerfaces 167: 8-19, 2018.

23. Jiang S, Han J, Li T, Xin Z, Ma Z, Di W, Hu W, Gong B, Di S, Wang D and Yang Y: Curcumin as a potential protective compound against cardiac diseases. Pharmacol Res 119: 373-383, 2017.
24. Zhao G, Liu Y, Yi X, Wang Y, Qiao S, Li Z, Ni J and Song Z: Curcumin inhibiting Th17 cell differentiation by regulating the metabotropic glutamate receptor-4 expression on dendritic cells. Int Immunopharmacol 46: 80-86, 2017.
25. Qi Z, Wu M, Fu Y, Huang T, Wang T, Sun Y, Feng Z and Li C: Palmitic acid curcumin ester facilitates protection of neuroblastoma against oligomeric aβ40 insult. Cell Physiol Biochem 44: 618-633, 2017.
26. Ren J and Sowers JR: Application of a novel curcumin analog in the management of diabetic cardiomyopathy. Diabetes 63: 3166-3168, 2014.
27. Li K, Liu Y, Zhang S, Xu Y, Jiang J, Yin F, Hu Y, Han B, Ge S, Zhang L and Wang Y: Folate receptor-targeted ultrasonic PFOB nanoparticles: Synthesis, characterization and application in tumor-targeted imaging. Int J Mol Med 39: 1505-1515, 2017.
28. Jiang X, Zhong Y, Zheng L and Zhao J: Nano-hydroxyapatite/collagen film as a favorable substrate to maintain the phenotype and promote the growth of chondrocytes cultured *in vitro*. Int J Mol Med 41: 2150-2158, 2018.
29. Jiang C, Wang H, Zhang X, Sun Z, Wang F, Cheng J, Xie H, Yu B and Zhou L: Deoxycholic acid-modified chitooligosaccharide/mPEG-PDLLA mixed micelles loaded with paclitaxel for enhanced antitumor efficacy. Int J Pharm 475: 60-68, 2014.
30. Chen Q, Pang MH, Ye XH, Yang G and Lin C: The toxoplasma gondii ME-49 strain upregulates levels of A20 that inhibit NF-κB activation and promotes apoptosis in human leukaemia T-cell lines. Parasite Vector 11: 305, 2018.
31. Shiomi M, Ishida T, Kobayashi T, Nitta N, Sonoda A, Yamada S, Koike T, Kuniyoshi N, Murata K, Hirata K, *et al*: Vasospasm of atherosclerotic coronary arteries precipitates acute ischemic myocardial damage in myocardial infarction-prone strain of the watanabe heritable hyperlipidemic rabbits. Arterioscler Thromb Vasc Biol 33: 2518-2523, 2013.
32. Li TB, Zhang YZ, Liu WQ, Zhang JJ, Peng J, Luo XJ and Ma QL: Correlation between NADPH oxidase-mediated oxidative stress and dysfunction of endothelial progenitor cell in hyperlipidemic patients. Korean J Intern Med 33: 313-322, 2018.
33. Yang SM, Liu J and Li CX: Intermedin protects against myocardial ischemia-reperfusion injury in hyperlipidemia rats. Genet Mol Res 13: 8309-8319, 2014.
34. Vendrov AE, Vendrov KC, Smith A, Yuan J, Sumida A, Robidoux J, Runge MS and Madamanchi NR: NOX4 NADPH oxidase-dependent mitochondrial oxidative stress in aging-associated cardiovascular disease. Antioxid Redox Signal 23: 1389-1409, 2015.
35. Lucas ML, Carraro CC, Bello-Klein A, Kalil AN, Aerts NR, Carvalho FB, Fernandes MC and Zettler CG: Oxidative stress in aortas of patients with advanced occlusive and aneurysmal diseases. Ann Vasc Surg 52: 216-224, 2018.
36. Murugesu K, Murugaiyah V, Saghir SAM, Asmawi MZ and Sadikun A: Caffeoylquinic acids rich versus poor fractions of gynura procumbens: Their comparative antihyperlipidemic and antioxidant potential. Curr Pharm Biotechnol 18: 1132-1140, 2017.
37. Hadzi-Petrushev N, Bogdanov J, Krajoska J, Ilievska J, Bogdanova-Popov B, Gjorgievska E, Mitrokhin V, Sopi R, Gagov H, Kamkin A and Mladenov M: Comparative study of the antioxidant properties of monocarbonyl curcumin analogues C66 and B2BrBC in isoproteranol induced cardiac damage. Life Sci 197: 10-18, 2018.
38. Li TB, Zhang JJ, Liu B, Luo XJ, Ma QL and Peng J: Dysfunction of endothelial progenitor cells in hyperlipidemic rats involves the increase of NADPH oxidase derived reactive oxygen species production. Can J Physiol Pharmacol 95: 474-480, 2017.
39. Lei S, Sun RZ, Wang D, Gong MZ, Su XP, Yi F and Peng ZW: Increased hepatic fatty acids uptake and oxidation by LRPPRC-driven oxidative phosphorylation reduces blood lipid levels. Front Physiol 7: 270, 2016.
40. Fan HC, Fernandez-Hernando C and Lai JH: Protein kinase C isoforms in atherosclerosis: Pro- or anti-inflammatory? Biochem Pharmacol 88: 139-149, 2014.
41. Chiu CJ and Taylor A: Dietary hyperglycemia, glycemic index and metabolic retinal diseases. Prog Retin Eye Res 30: 18-53, 2011.
42. Yang R, Chu X, Sun L, Kang Z, Ji M, Yu Y, Liu Y, He Z and Gao N: Hypolipidemic activity and mechanisms of the total phenylpropanoid glycosides from ligustrum robustum (Roxb.) Blume by AMPK-SREBP-1c pathway in hamsters fed a high-fat diet. Phytother Res 32: 715-722, 2018.
43. Lin CH, Kuo YH and Shih CC: Effects of bofu-tsusho-san on diabetes and hyperlipidemia associated with AMP-activated protein kinase and glucosetransporter 4 in high-fat-fed mice. Int J Mol Sci 15: 20022-20044, 2014.
44. Vinayagam R, Jayachandran M, Chung SSM and Xu B: Guava leaf inhibits hepatic gluconeogenesis and increases glycogen synthesis via AMPK/ACC signaling pathways in streptozotocin-induced diabetic rats. Biomed Pharmacother 103: 1012-1017, 2018.
45. Yeung PK, Kolathuru SS, Mohammadizadeh S, Akhoundi F and Linderfield B: Adenosine 5'-triphosphate metabolism in red blood cells as a potential biomarker for post-exercise hypotension and a drug target for cardiovascular protection. Metabolites 8: E30, 2018.
46. Mollica MP, Mattace Raso G, Cavaliere G, Trinchese G, De Filippo C, Aceto S, Prisco M, Pirozzi C, Di Guida F, Lama A, *et al*: Butyrate regulates liver mitochondrial function, efficiency, and dynamics in insulin-resistant obese mice. Diabetes 66: 1405-1418, 2017.
47. Li Y, Zhou ZH, Chen MH, Yang J, Leng J, Cao GS, Xin GZ, Liu LF, Kou JP, Liu BL, *et al*: Inhibition of mitochondrial fission and NOX2 expression prevent NLRP3 inflammasome activation in the endothelium: The role of corosolic acid action in the amelioration of endothelial dysfunction. Antioxid Redox Signal 24: 893-908, 2016.
48. Lone J, Choi JH, Kim SW and Yun JW: Curcumin induces brown fat-like phenotype in 3T3-L1 and primary white adipocytes. J Nutr Biochem 27: 193-202, 2016.
49. Pu Y, Zhang H, Wang P, Zhao Y, Li Q, Wei X, Cui Y, Sun J, Shang Q, Liu D and Zhu Z: Dietary curcumin ameliorates aging-related cerebrovascular dysfunction through the AMPK/uncoupling protein 2 pathway. Cell Physiol Biochem 32: 1167-1177, 2013.
50. Yang K, Xu C, Li X and Jiang H: Combination of D942 with curcumin protects cardiomyocytes from ischemic damage through promoting autophagy. J Cardiovasc Pharmacol Ther 18: 570-581, 2013.
51. Mikhailov V, Mikhailova M, Pulkrabek DJ, Dong Z, Venkatachalam MA and Saikumar P: Bcl-2 prevents Bax oligomerization in the mitochondrial outer membrane. J Biol Chem 276: 18361-18374, 2001.